Research Square

Preprints are preliminary reports that have not undergone peer review.
They should not be considered conclusive, used to inform clinical practice,
or referenced by the media as validated information.

Longitudinal multimodal MRI assessment of glymphatic changes after subthalamic nucleus deep brain stimulation in Parkinson disease

Peng CHEN
University of Science and Technology of China
Chi XIONG
University of Science and Technology of China
Manli JIANG
University of Science and Technology of China
Yuanfei WANG
University of Science and Technology of China
Ce ZHANG
University of Science and Technology of China
Shanshan WANG
University of Science and Technology of China
Hu HE
University of Science and Technology of China
Jianmin SI
University of Science and Technology of China
Chaoshi NIU
niuchaoshi@ustc.edu.cn

University of Science and Technology of China

Article

Keywords: Parkinson's disease, STN-DBS, glymphatic system, gBOLD-CSF coupling, DTI-ALPS, perivascular spaces, sleep, multimodal MRI

Posted Date: November 4th, 2026

DOI: https://doi.org/10.21203/rs.3.rs-11231286/v1

License: This work is licensed under a Creative Commons Attribution 4.0 International License.
Read Full License

Additional Declarations: No competing interests reported.

Abstract

Effects of subthalamic nucleus deep brain stimulation (STN-DBS) on glymphatic-related MRI markers in Parkinson disease (PD) are unclear. We conducted a longitudinal multimodal MRI study on 38 patients with PD who underwent bilateral STN-DBS with a 3T MRI-compatible DBS system and completed paired preoperative and one-year postoperative imaging. Three MRI-derived glymphatic-related markers were evaluated: global BOLD-CSF coupling strength, diffusion tensor imaging along the perivascular space (DTI-ALPS), and MRI-visible perivascular space (PVS) count. gBOLD-CSF coupling strength increased (95% CI, 0.021-0.200; P = 0.0173) significantly after STN-DBS, whereas DTI-ALPS and PVS count did not show statistically significant longitudinal changes. Greater postoperative enhancement of gBOLD-CSF coupling was associated with greater improvement in Parkinson Disease Sleep Scale scores (Spearman rho = 0.531, P = 0.0006; FDR q = 0.0048) and showed a nominal association with LEDD reduction (Spearman rho = 0.389, P = 0.0159; FDR q = 0.0636). In contrast, longitudinal changes in DTI-ALPS and PVS count were not significantly associated with clinical improvement. These findings suggest that functional BOLD-CSF coupling may be a sensitive MRI marker of postoperative glymphatic-related change after STN-DBS.

Introduction

Parkinson's disease (PD) is a progressive neurodegenerative disorder characterized pathologically by dopaminergic neuronal loss and alpha-synuclein aggregation, and clinically by both motor and non-motor manifestations[1]. Subthalamic nucleus deep brain stimulation (STN-DBS) is an established therapy for appropriately selected patients with advanced PD and improves motor symptoms while reducing dopaminergic medication requirements[2,3]. However, non-motor symptoms, including sleep disturbance, mood symptoms, cognitive impairment, autonomic dysfunction, and impaired quality of life, remain major contributors to disability and postoperative outcome variability[4,5].

The glymphatic system has emerged as a brain wide pathway that supports cerebrospinal fluid (CSF)-interstitial fluid exchange and clearance of soluble interstitial solutes in experimental models[6]. Foundational mouse work linked sleep and anesthesia to expansion of interstitial space and enhanced tracer clearance, although subsequent experimental work indicates that clearance can vary by tracer, state, and methodology and should not be assumed to be uniformly increased during sleep[7,8]. In humans, simultaneous neurophysiological and MRI measurements have shown coupled electrophysiological, hemodynamic, and CSF oscillations during non-rapid eye movement sleep, providing a physiologic basis for MRI-derived BOLD-CSF coupling analyses[9].

Several lines of evidence suggest that glymphatic and meningeal lymphatic dysfunction may be relevant to PD. Human imaging and experimental studies have reported impaired meningeal lymphatic drainage in idiopathic PD and worsening of PD-like alpha-synuclein pathology after blockade of meningeal lymphatic drainage in mice[10,11]. MRI-based approaches have been developed to interrogate glymphatic-related physiology indirectly. The DTI-ALPS index was introduced as a diffusion MRI method intended to

estimate water diffusivity along medullary perivascular spaces[12], and several PD studies have reported reduced ALPS indices or associations with disease severity, cognition, or progression[13–15]. MRI-visible PVS burden has also been associated with cognitive decline and regional perivascular-space changes in PD[16,17]. In parallel, lagged coupling between global BOLD activity and CSF inflow has been proposed as an indirect functional marker of brain-fluid dynamics and has been linked to neurodegenerative pathology and clinical features in AD and PD cohorts[18–20].

Despite these advances, important gaps remain. First, most glymphatic-related MRI studies in PD have been cross-sectional, limiting inference about whether these abnormalities are modifiable after effective treatment[13–20]. Second, many studies have relied on a single imaging marker, although DTI-ALPS, BOLD-CSF coupling, and MRI-visible PVS quantify different, indirect aspects of tissue diffusivity, functional CSF signal dynamics, and structural perivascular-space burden. Third, emerging validation work cautions that DTI-ALPS is influenced by local diffusion geometry and does not provide a direct measure of glymphatic solute clearance[21,22]. Because STN-DBS can improve sleep and other non-motor symptoms in PD[23,24], it provides a clinically relevant context in which to examine whether glymphatic-related MRI markers change after intervention.

This study was designed to address these gaps by using a longitudinal multimodal MRI framework to characterize glymphatic-related changes in PD patients before and one year after STN-DBS. We integrated three complementary MRI markers: functional global BOLD-CSF coupling strength, diffusion-based DTI-ALPS, and structural PVS count. We further examined whether postoperative changes in these markers were associated with changes in sleep, motor symptoms, medication burden, non-motor symptoms, quality of life, mood, and cognition. We hypothesized that STN-DBS would be associated with postoperative modulation of glymphatic-related MRI markers and that imaging changes would be related particularly to improvement in sleep and overall non-motor status.

Results

Study cohort and valid paired imaging data

A total of 38 patients with Parkinson’s disease had valid paired preoperative and one-year postoperative datasets for the primary longitudinal analyses. All 38 patients had available paired resting-state fMRI data for global BOLD-CSF coupling analysis, paired diffusion MRI data for mean bilateral DTI-ALPS analysis, matched PVS count data, and complete clinical change scores. The cohort included 20 men and 18 women, with a mean age of 56.76 ± 5.04 years, disease duration of 8.97 ± 3.94 years, and Hoehn and Yahr stage of 3.0 [3.0, 4.0]. Participant characteristics are shown in Table 1 and Supplementary Table S1.

Table 1
Baseline demographic, clinical assessments and glymphatic-related markers.

Characteristic	Preoperative	Postoperative	Paired t P
Age, years	56.8 ± 5.0		
Sex, male	20 (52.6)		
Sex, female	18 (47.4)		
Disease duration, years	9.0 ± 3.9		
Hoehn and Yahr stage	3.0 [3.0, 4.0]		
LEDD, mg/day	670.1 ± 254.4	388.4 ± 176.3	< 0.001
UPDRS-III score	48.9 ± 13.6	21.9 ± 8.9	< 0.001
NMSS score	54.6 ± 18.6	46.7 ± 20.2	0.056
PDQ-39 score	58.1 ± 17.5	47.1 ± 19.7	0.007
MMSE score	27.2 ± 2.9	27.4 ± 2.4	0.697
HAMD score	13.6 ± 5.2	10.2 ± 5.1	0.004
HAMA score	13.9 ± 4.2	9.2 ± 4.0	< 0.001
PDSS score	110.0 ± 13.0	120.7 ± 11.5	< 0.001
gBOLD–CSF coupling index (-r)	0.056 ± 0.188	0.166 ± 0.200	0.017
DTI-ALPS mean	1.163 ± 0.229	1.158 ± 0.258	0.927
PVS count	74.6 ± 62.2	62.7 ± 34.7	0.189

Data are mean (SD), median [IQR], or n (%), as appropriate (n = 38).LEDD, Levodopa equivalent daily dose; Movement Disorder Society Unified Parkinson's Disease Rating Scale; NMSS, Non-Motor Symptoms Scale; PDQ-39, Parkinson's Disease Questionnaire-39; MMSE, Mini-Mental State Examination UPDRS; HAMA, Hamilton Anxiety Rating Scale; HAMD, Hamilton Depression Rating Scale, PDSS, Parkinson's Disease Sleep Scale score; DTI-ALPS, diffusion tensor imaging along the perivascular space; PVS, perivascular space.

Postoperative enhancement of gBOLD-CSF coupling strength

Global BOLD-CSF coupling strength showed a significant postoperative increase at one year after STN-DBS. The mean preoperative coupling strength was 0.056 ± 0.188, whereas the mean postoperative coupling strength was 0.166 ± 0.200. The mean postoperative change was + 0.110 ± 0.273, indicating an overall enhancement of gBOLD-CSF coupling strength after surgery. This increase was statistically significant using both the paired t-test and the Wilcoxon signed-rank test (paired t-test, P = 0.0173; Wilcoxon test, P = 0.0253). The estimated 95% confidence interval for the mean change was 0.021 to

0.200, with a paired effect size of Cohen's dz = 0.40. Details are shown in Table 1, Supplementary Table S2 and Fig. 2B-E.

At the individual level, 25 of 38 patients (65.8%) showed increased postoperative gBOLD-CSF coupling strength, whereas 13 patients (34.2%) showed decreased coupling strength. Because coupling strength was directionally oriented as the negative of the raw r(+ 4 s) value, the raw r(+ 4 s) measure showed the opposite pattern. The mean raw r(+ 4 s) became more negative, changing from − 0.056 ± 0.188 before surgery to -0.166 ± 0.200 after surgery, with a mean change of -0.110 ± 0.273. This change was significant using both paired tests (paired t-test, P = 0.0173; Wilcoxon test, P = 0.0253), consistent with the observed enhancement in directionally oriented gBOLD-CSF coupling strength. Details are shown in Fig. 2F, G.

Association between gBOLD-CSF coupling change and clinical improvement

Delta gBOLD-CSF coupling strength was significantly positively correlated with PDSS improvement, indicating that patients with greater enhancement of BOLD-CSF coupling tended to have greater postoperative sleep improvement (Spearman rho = 0.531, P = 0.0006; FDR q = 0.0048). Delta gBOLD-CSF coupling strength was also nominally correlated with LEDD reduction (Spearman rho = 0.389, P = 0.0159; FDR q = 0.0636). In contrast, delta gBOLD-CSF coupling strength was not significantly associated with UPDRS-III improvement (Spearman rho = -0.112, P = 0.5019). No significant associations were observed with NMSS improvement, PDQ-39 improvement, MMSE change, HAMD improvement, or HAMA improvement in the primary Spearman analyses. Details are shown in Fig. 3 and Supplementary Table S3.

The association with sleep improvement remained robust after adjustment for age, sex, and disease duration. In partial Spearman correlation analyses, delta gBOLD-CSF coupling strength remained significantly associated with PDSS improvement (partial r = 0.560, P = 0.0005, FDR q = 0.0038). The association with LEDD reduction remained nominal after adjustment (partial r = 0.390, P = 0.0206, FDR q = 0.0823). Additional sensitivity analyses further adjusting for Hoehn and Yahr stage yielded similar results for PDSS improvement (partial r = 0.562, P = 0.0005) and a nominal association with LEDD reduction (partial r = 0.390, P = 0.0228), whereas the association with UPDRS-III improvement remained non-significant (partial r = -0.113, P = 0.5249). Details are shown in Fig. 3 and Supplementary Table S4-6.

DTI-ALPS showed no significant postoperative change

DTI-ALPS indices did not show significant longitudinal changes after STN-DBS. The mean bilateral ALPS index was 1.163 ± 0.229 before surgery and 1.158 ± 0.258 after surgery, with a mean change of -0.005 ± 0.332. This change was not statistically significant using either the paired t-test or Wilcoxon signed-rank test (paired t-test, P = 0.927; Wilcoxon test, P = 0.720). At the individual level, 19 patients showed

increased ALPS Mean and 19 showed decreased ALPS Mean. Details are shown in Table 1 and Supplementary Table S2.

Correlation analyses further showed that delta ALPS Mean was not significantly associated with clinical improvement. Delta ALPS Mean showed no significant association with PDSS improvement (Spearman rho = 0.044, P = 0.7950), LEDD reduction (rho = 0.174, P = 0.2968), or UPDRS-III improvement (rho = -0.069, P = 0.6793). No significant associations were observed with NMSS improvement, PDQ-39 improvement, MMSE change, HAMD improvement, or HAMA improvement. Adjustment for age, sex, and disease duration did not reveal significant associations between delta ALPS Mean and clinical outcomes. Details are shown in Fig. 4 and Supplementary Table S4-6.

PVS count showed a non significant postoperative decrease

PVS count showed a numerical decrease after STN-DBS but did not reach statistical significance. The mean preoperative PVS count was 74.63 ± 62.23, whereas the mean postoperative PVS count was 62.71 ± 34.67. The mean postoperative change was − 11.92 ± 54.90, with an estimated 95% confidence interval from − 29.97 to 6.13, indicating a trend toward reduced PVS count that did not reach statistical significance (paired t-test, P = 0.1889; Wilcoxon test, P = 0.9699). Details are shown in Table 1 and Supplementary Table S2.

Delta PVS count was not significantly associated with clinical improvement. In key outcome analyses, delta PVS count was not associated with PDSS improvement (Spearman rho = 0.082, P = 0.6266), LEDD reduction (rho = -0.015, P = 0.9301), or UPDRS-III improvement (rho = -0.146, P = 0.3805). No significant correlations were observed between delta PVS count and NMSS improvement, PDQ-39 improvement, MMSE change, HAMD improvement, or HAMA improvement. No association involving PVS count survived FDR correction across the broader clinical correlation analyses. Details are shown in Fig. 5 and Supplementary Table S4-6.

Integrated multimodal signature of glymphatic-related MRI changes

Among the 38 participants with paired data, gBOLD-CSF coupling increased after STN-DBS, with a standardized paired effect size of 0.404 (Cohen’s d; 95% bootstrap CI, 0.094 to 0.752). The corresponding effect estimates were − 0.015 for mean DTI-ALPS (95% bootstrap CI, -0.358 to 0.299) and − 0.217 for PVS count (95% bootstrap CI, -0.471 to 0.093), with both confidence intervals spanning zero (Figure. 6A).

In exploratory, unadjusted Spearman analyses, greater increases in gBOLD-CSF coupling were associated with greater PDSS improvement (ρ = 0.531, P < 0.001) and LEDD reduction (ρ = 0.389, P = 0.016). No statistically significant association was detected with UPDRS-III improvement (ρ = -0.112, P =

0.502). Changes in mean DTI-ALPS and PVS count were not significantly correlated with any of the three clinical outcomes (all $|\rho| \leq 0.174$; all $P \geq 0.297$; Figure. 6B). Details are shown in Supplementary Table S3.

Discussion

In this longitudinal multimodal MRI study of patients with PD undergoing bilateral STN-DBS, we investigated postoperative changes in three complementary glymphatic-related MRI markers: functional gBOLD-CSF coupling strength, diffusion-based DTI-ALPS, and structural PVS count. The principal findings were that gBOLD-CSF coupling strength significantly increased one year after STN-DBS, and that greater coupling enhancement was associated with greater sleep improvement and nominally with medication reduction, but not with motor improvement. In contrast, DTI-ALPS and PVS count showed no significant postoperative change. Longitudinal changes in ALPS and PVS count were not significantly associated with key clinical outcomes. These results suggest that functional BOLD-CSF coupling may be more sensitive than diffusion-based or structural markers for capturing postoperative glymphatic-related changes after STN-DBS.

Functional BOLD-CSF coupling as a sensitive postoperative marker

The most responsive imaging finding was the postoperative enhancement of gBOLD-CSF coupling strength. This measure captures the temporal relationship between global brain activity, hemodynamic fluctuations, and CSF signal changes, and has been interpreted as an indirect functional marker of brain-fluid dynamics rather than a direct measurement of solute clearance[9,18–20]. In this cohort, gBOLD-CSF coupling increased significantly after STN-DBS, whereas ALPS and PVS count did not. These findings suggest that coupling-based fMRI metrics may be more sensitive to dynamic postoperative physiologic changes than diffusion-derived or structural PVS measures.

The distribution of delta gBOLD-CSF coupling strength was shifted toward positive mean values, with approximately two thirds of patients showing postoperative enhancement. This pattern indicates heterogeneity in individual coupling responses after STN-DBS. The paired effect size was small to moderate, and the result was significant in both parametric and non-parametric paired testing. Therefore, the strongest support for gBOLD-CSF coupling in this cohort comes from the convergence of a significant longitudinal mean shift and its consistent association with sleep improvement.

Association with sleep improvement and medication reduction

A key clinical observation was that coupling enhancement was associated with PDSS improvement. This association remained significant after adjustment for age, sex, and disease duration and persisted in sensitivity analyses accounting for LEDD change. Because sleep, neural activity, vascular oscillations, and CSF dynamics are physiologically linked[7–9], improvement in sleep after STN-DBS may plausibly

relate to altered BOLD-CSF coupling. However, the present observational design cannot determine whether sleep improvement drives coupling enhancement, whether coupling changes contribute to sleep improvement, or whether both reflect broader postoperative physiologic changes. Prior DBS studies support the clinical plausibility of postoperative sleep improvement in PD[23,24].

Delta gBOLD-CSF coupling strength was also nominally associated with LEDD reduction. This association should be interpreted as treatment-related rather than causal, because medication reduction is influenced by programming strategy, physician decision-making, and individual tolerability. Nevertheless, the finding suggests that patients with greater functional coupling enhancement tended to show greater postoperative reduction in dopaminergic medication burden. The absence of a significant association with UPDRS-III improvement is notable and suggests that gBOLD-CSF coupling does not simply mirror motor circuit improvement. Instead, it may capture a distinct postoperative dimension related to sleep, arousal regulation, medication burden, and brain fluid dynamics.

Why DTI-ALPS and PVS showed weaker longitudinal sensitivity

DTI-ALPS and PVS count showed weaker postoperative signals than gBOLD-CSF coupling. The absence of a significant ALPS change does not contradict previous cross-sectional studies reporting lower ALPS index in PD or associations with progression, because cross-sectional differences may reflect chronic tissue or vascular properties rather than short-term postoperative change[13–15]. In addition, recent validation and simulation work indicates that DTI-ALPS should not be treated as a direct or biologically specific marker of glymphatic clearance, because it can be influenced by local fiber geometry and directional diffusivity unrelated to perivascular clearance[21,22].

Similarly, PVS count is a structural marker that may represent relatively chronic perivascular-space enlargement rather than dynamic fluid exchange[25]. Although MRI-visible PVS burden has been associated with cognitive decline and regional PVS abnormalities in PD[16,17], the non-significant postoperative decrease observed here suggests that PVS count may be less sensitive to one-year postoperative functional change than gBOLD-CSF coupling.

Implications for glymphatic-related imaging after DBS

The comparative pattern across modalities has methodological and biological implications. A single MRI marker is unlikely to capture the full complexity of glymphatic-related physiology. gBOLD-CSF coupling, DTI-ALPS, and PVS count measure different proxy domains: dynamic coupling between global BOLD and CSF signals, directional diffusion along perivascular regions, and structural perivascular-space burden, respectively[12,18,20,25]. Their divergent longitudinal behavior in this study may therefore reflect differences in temporal sensitivity, biological specificity, and susceptibility to postoperative confounds.

These findings should be framed as glymphatic-related rather than as direct proof of glymphatic restoration. The term "glymphatic-related" is important because none of the MRI measures used here

directly quantifies solute clearance, aquaporin-4 polarization, meningeal lymphatic outflow, or interstitial-fluid turnover. Current validation studies support cautious interpretation of MRI proxies, particularly DTI-ALPS, and discourage assigning biological specificity beyond what the method can establish[21,22]. Finally, we propose a potential mechanistic framework for linking STN-DBS to glymphatic-related MRI changes (Fig. 6C).

Strengths and limitations

The strengths of this study include its longitudinal within-subject design, integration of functional, diffusion-based, and structural MRI markers, and assessment of multiple clinical domains relevant to postoperative outcomes. The paired design reduced inter-individual variability and allowed direct estimation of postoperative change. The use of artifact control and valid brain masks in postoperative rs-fMRI analysis was also important given the technical challenges of imaging patients after DBS.

Several limitations should be acknowledged. First, the sample size was modest, and the findings require validation in larger cohorts. Second, the study did not include a non-surgical PD control group or a healthy longitudinal control group, limiting causal inference regarding DBS-specific effects. Third, MRI-derived glymphatic-related markers are indirect proxies, and recent work highlights important methodological constraints, especially for DTI-ALPS[21,22]. Fourth, postoperative DBS artifacts and stimulation-related changes in brain state may influence imaging measurements despite artifact masking and quality control. Fifth, sleep was assessed clinically rather than with polysomnography or actigraphy, preventing direct assessment of sleep architecture or slow-wave activity. Finally, the follow-up interval was limited to one year, and longer longitudinal studies are needed to determine whether gBOLD-CSF coupling changes persist and whether they predict long-term clinical outcomes.

Conclusions

In conclusion, this longitudinal multimodal MRI study showed that gBOLD-CSF coupling strength increased one year after STN-DBS in patients with PD. Coupling enhancement was associated with sleep improvement and nominally with medication reduction, but not with motor improvement. In contrast, DTI-ALPS and PVS count showed limited postoperative change and weak clinical associations. These findings suggest that functional BOLD-CSF coupling may be a sensitive glymphatic-related imaging marker of postoperative sleep-related and treatment-related benefit after STN-DBS, while structural and diffusion-based markers may be less responsive over a one-year follow-up period.

Materials and Methods

Study design and participants

This was a longitudinal multimodal MRI study of patients with Parkinson’s disease (PD) who underwent bilateral subthalamic nucleus deep brain stimulation (STN-DBS). All participants completed MRI and

clinical assessments before surgery and at approximately one year after DBS. The primary objective was to characterize postoperative changes in glymphatic-related MRI markers, including global BOLD-CSF coupling, diffusion tensor image analysis along the perivascular space (DTI-ALPS), and MRI-visible perivascular space (PVS) burden. The secondary objective was to determine whether longitudinal changes in these imaging markers were associated with postoperative clinical improvement. Details are shown in Fig. 1.

Patients were recruited from the Department of Neurosurgery, the First Affiliated Hospital of USTC, between October 2022 and May 2025. PD was diagnosed according to the Movement Disorder Society clinical diagnostic criteria[26]. All patients fulfilled institutional criteria for bilateral STN-DBS, including clinically established PD, levodopa responsiveness, disabling motor fluctuations or medication-refractory tremor, and multidisciplinary evaluation consistent with expert DBS selection principles[27]. Further details can be found in the Supplementary Methods 1.

Of 50 screened patients, 12 were excluded because of absence of preoperative T1-weighted imaging (n = 5), incomplete diffusion-weighted imaging data (n = 3), excessive head motion or imaging artefacts (n = 4). A total of 38 patients with valid paired preoperative and postoperative MRI datasets were included in the final analysis. All participants provided written informed consent. The study was approved by the institutional ethics committee and conducted in accordance with the Declaration of Helsinki[28].

DBS surgery and postoperative follow-up

All patients underwent bilateral STN-DBS using a standard stereotactic procedure consistent with established DBS practice for PD[27]. The surgical target was planned on preoperative MRI and refined according to individual anatomical landmarks. Intraoperative microelectrode recording and/or test stimulation were used according to institutional practice. Permanent electrodes were implanted bilaterally in the STN and connected to an implantable pulse generator. Each component of the 3T MRI-compatible DBS system received approval from the National Medical Products Administration of China, formerly known as the China Food and Drug Administration. For the DBS system, stimulation can be turned on or off during MRI. Further details can be found in the Supplementary Methods 1.

Clinical and MRI follow-up assessments were performed approximately one year after surgery. Postoperative clinical assessments were conducted in the stimulation-on state under the patient's optimized programming settings. Dopaminergic medication was adjusted after DBS according to clinical response and tolerability, and levodopa equivalent daily dose (LEDD) was calculated using established conversion recommendations[29].

Clinical assessments

Clinical evaluations were performed before surgery and at one-year postoperative follow-up. Motor severity was assessed using the Unified Parkinson's Disease Rating Scale part III (UPDRS-III)[30]. Disease severity was assessed with Hoehn and Yahr staging[31]. Non-motor symptoms were evaluated using the

Non-Motor Symptoms Scale (NMSS)[32], quality of life using the Parkinson's Disease Questionnaire-39 (PDQ-39)[33], global cognition using the Mini-Mental State Examination (MMSE)[34], depressive symptoms using the Hamilton Depression Rating Scale (HAMD)[35], anxiety symptoms using the Hamilton Anxiety Rating Scale (HAMA)[36], and sleep symptoms using the Parkinson's Disease Sleep Scale (PDSS)[37]. Dopaminergic medication burden was expressed as LEDD[29].

Clinical change scores were calculated to represent postoperative improvement. For scales in which lower scores indicate better clinical status, including UPDRS-III, NMSS, PDQ-39, HAMD, HAMA, and LEDD, improvement was calculated as preoperative value minus postoperative value. For scales in which higher scores indicate better status, including PDSS and MMSE, change was calculated as postoperative value minus preoperative value. Thus, positive change scores consistently represented clinical improvement or medication reduction.

MRI acquisition

MRI data were acquired before surgery and at one-year postoperative follow-up using a 3.0-T MRI scanner (GE Discovery MR750) with a 8-channel head coil. The multimodal MRI protocol included high-resolution three-dimensional T1-weighted imaging, diffusion-weighted imaging for DTI-ALPS analysis, and resting-state functional MRI for BOLD-CSF coupling analysis.

Three dimensional T1-weighted images were acquired using a magnetisation prepared rapid gradient echo sequence (repetition time, 8.6 ms; echo time, 3.2 ms; inversion time, 450 ms; flip angle, 12°; field of view, 256 × 256 mm^2; matrix, 256 × 256; slice thickness, 1 mm; isotropic voxel size, 1 × 1 × 1 mm^3). Diffusion imaging included b = 0 and b = 1000 s/mm^2 acquisitions with 64 diffusion encoding directions (repetition time, 15059 ms; echo time, 96 ms; matrix, 128 × 128; slice thickness, 2 mm).

For resting-state functional MRI: repetition time = 2000 ms, echo time = 30 ms, flip angle = 90°, voxel size = 3.75 × 3.75 × 4.10 mm^3, field of view = 240mm × 240mm, and resulting in a total acquisition duration of approximately 6 min 44 s. During resting-state scanning, participants were instructed to keep their eyes closed, remain awake, stay still, and not think of anything in particular.

All MRI data underwent visual quality control. Datasets with excessive motion, incomplete brain coverage, major artifacts, or failed registration were excluded from analysis. Only patients with valid paired preoperative and postoperative datasets were retained for the final analysis.

Structural MRI preprocessing

T1-weighted images were processed in a longitudinal framework. First, each T1-weighted image underwent intensity nonuniformity correction, skull stripping, and tissue segmentation into gray matter, white matter, and CSF using established structural MRI processing methods[38,39]. For each participant, preoperative and postoperative scans were processed using an unbiased within-subject longitudinal template to improve consistency across time points[40]. Images were registered to individual and

standard spaces using nonlinear registration procedures consistent with symmetric diffeomorphic registration approaches[41].

Structural preprocessing quality control included visual inspection of skull stripping, pial and white-matter surfaces, segmentation boundaries, and registration accuracy. Scans with major failure were either manually corrected according to FreeSurfer recommendations or excluded if acceptable recovery was not possible. Structural outputs were primarily used for anatomical characterization, covariate extraction, and cross-modal registration of diffusion and rs-fMRI data.

Resting-state fMRI preprocessing

Resting-state fMRI data were preprocessed using (FSL; https://fsl.fmrib.ox.ac.uk/fsl/docs/)[42]. The preprocessing steps included removal of the initial volumes, slice-timing correction, realignment for head-motion correction, co-registration to individual structural images, normalization, spatial smoothing, and temporal filtering. Motion parameters and framewise displacement were calculated to characterize head motion, given the known impact of motion on resting-state fMRI correlations[43]. Nuisance regression included motion parameters, white matter signal, CSF signal outside the target inflow region, and other confound regressors according to the predefined preprocessing pipeline.

For postoperative scans, special attention was paid to DBS-related artifacts. Individual postoperative artifact masks were generated when necessary, and analyses were restricted to valid brain voxels to reduce the influence of stimulation lead-related signal dropout or distortion. A common valid mask was used to ensure that preoperative and postoperative gBOLD-CSF coupling measures were extracted from comparable brain regions. Further details can be found in the Supplementary Methods 2 and Supplementary Fig. 1.

gBOLD-CSF coupling analysis

Global BOLD-CSF coupling was calculated from preprocessed resting-state fMRI data using a previously described lagged cross-correlation approach[9,18,20]. Briefly, a global gray matter BOLD signal was extracted from the valid brain mask. A CSF inflow signal was extracted from a region of interest in the inferior slice or ventricular/subarachnoid CSF space, following prior BOLD-CSF coupling analyses. Both signals were detrended and standardized before cross-correlation analysis.

Lagged cross-correlation between the global BOLD signal and CSF signal was calculated across a predefined temporal lag window. Based on the temporal resolution of the resting-state fMRI sequence and prior PD work on BOLD-CSF coupling, the correlation coefficient at + 4 seconds, r(+ 4 s), was selected as the primary coupling metric[20]. Because stronger BOLD-CSF coupling is expressed as a more negative r(+ 4 s) value in this framework, coupling strength was defined as -r(+ 4 s), so that higher values indicated stronger coupling. Further details can be found in the Supplementary Methods 3.

Delta gBOLD-CSF coupling strength = postoperative coupling strength - preoperative coupling strength. Patients were further classified according to the direction of change as Post > Pre or Post < Pre.

DTI preprocessing and DTI-ALPS analysis

Diffusion MRI data were preprocessed using (DSI Studio; Chen May 17 2024 version). Preprocessing included correction for eddy-current distortion and head motion, brain extraction, and diffusion tensor fitting using established diffusion MRI methods[42,44,45]. Diffusion maps, including directional diffusivity maps along the x-, y-, and z-axes, were generated for ALPS calculation.

DTI-ALPS analysis was performed on preoperative and postoperative diffusion images using manually defined regions of interest in the periventricular white matter at the level of the lateral ventricles, following the original DTI-ALPS method[12]. Projection and association fiber regions were identified on color-coded fractional anisotropy maps. Directional diffusivities were extracted from projection and association regions in each hemisphere. ALPS-index was calculated as: ALPS-index=mean(Dxx,proj,Dxx,assoc)/mean(Dyy,proj,Dzz,assoc).

The primary DTI-ALPS longitudinal metric was Delta ALPS Mean, calculated as postoperative ALPS Mean minus preoperative ALPS Mean. Further details can be found in the Supplementary Methods 4.

PVS count analysis

MRI-visible PVS burden was assessed on preoperative and postoperative structural MRI using a predefined PVS quantification pipeline. Images were first aligned to the individual anatomical space and visually inspected for quality. PVS were identified as small CSF-like linear or punctate structures following established MRI descriptions of perivascular spaces, and image-processing methods were applied to enhance PVS visibility and quantification[25,46]. Total PVS count was calculated for each participant at each time point. Further details can be found in the Supplementary Methods 5.

The primary structural PVS metric was total PVS count. Longitudinal change in PVS burden was defined as: Delta PVS count = postoperative PVS count - preoperative PVS count. A negative Delta PVS count indicated a reduction in PVS burden after DBS, whereas a positive value indicated increased PVS burden.

Statistical analysis

Statistical analyses were performed using Python 3.10 and SPSS 23.0 Continuous variables were summarized as mean ± standard deviation or median with interquartile range, depending on distribution. Categorical variables were summarized as counts and percentages. Preoperative and postoperative imaging measures were compared using paired t tests for normally distributed variables and Wilcoxon signed-rank tests for non-normally distributed variables. The primary longitudinal imaging outcome was Delta gBOLD-CSF coupling strength. Secondary imaging outcomes included Delta ALPS Mean and Delta PVS count. The proportion of patients showing increased versus decreased gBOLD-CSF coupling strength was also calculated.

Associations between imaging markers and clinical change scores were assessed using Spearman correlation analysis as the primary approach, because several clinical and imaging variables were not normally distributed. Pearson correlation analyses were additionally performed as sensitivity analyses. Correlations were examined between preoperative, postoperative, and delta imaging markers and postoperative clinical improvement measures, including UPDRS-III improvement, LEDD reduction, PDSS improvement, NMSS improvement, PDQ-39 improvement, MMSE change, HAMD improvement, and HAMA improvement.

To account for potential confounding effects, partial Spearman correlation analyses were performed for key associations after adjusting for age, sex, and disease duration. Additional sensitivity analyses further adjusted for LEDD change and Hoehn and Yahr stage when examining imaging-clinical associations. Multiple-comparison correction was performed using the false discovery rate approach. Statistical significance was defined as two-sided $P < 0.05$.

Declarations

Author contributions: P.C. designed the research study, conducted experiments, acquired and analyzed data, wrote and edited the manuscript, and generated figures and tables; C.X. contributed imaging data acquisition, tabulation, and analysis; ML.J. contributed data acquisition, data analysis, and manuscript editing; YF.W. collected demographic and clinical data; C.Z. performed neurological examinations, acquired and analyzed data, and edited the manuscript; SS.W. provided patient care coordination, and acquired and analyzed data; H.H. conducting experiments, acquired demographic and clinical data, and analyzed data; JM.S. acquired and analyzed data and edited the manuscript; CS.N. developed and applied statistical methods, analyzed data, generated figures and tables, and wrote and edited the manuscript. All authors reviewed the manuscript.

Funding: The Excellent Research and Innovation Team Project of Anhui Province University, 2023AH010080; Fundamental Research Funds for the Central Universities, YD9110002037.

Competing interests: None declared.

Ethics approval: This study was approved by the institutional review board of the First Affiliated Hospital of USTC (Ethics Review No.2022-RE-154).

Data availability statement: Data generated or analyzed during the study are available from the corresponding author by request.

References

1. Bloem, B. R., Okun, M. S. & Klein, C. Parkinson's disease. Lancet 397, 2284–2303 (2021).
2. Deuschl, G. et al. A randomized trial of deep-brain stimulation for Parkinson's disease. N. Engl. J. Med. 355, 896–908 (2006).

3. Kleiner-Fisman, G. et al. Subthalamic nucleus deep brain stimulation: summary and meta-analysis of outcomes. Mov. Disord. 21 (Suppl. 14), S290–S304 (2006).
4. Chaudhuri, K. R., Healy, D. G. & Schapira, A. H. Non-motor symptoms of Parkinson's disease: diagnosis and management. Lancet Neurol. 5, 235–245 (2006).
5. Prakash, K. M., Nadkarni, N. V., Lye, W. K., Yong, M. H. & Tan, E. K. The impact of non-motor symptoms on the quality of life of Parkinson's disease patients: a longitudinal study. Eur. J. Neurol. 23, 854–860 (2016).
6. Iliff, J. J. et al. A paravascular pathway facilitates CSF flow through the brain parenchyma and the clearance of interstitial solutes, including amyloid beta. Sci. Transl. Med. 4, 147ra111 (2012).
7. Xie, L. et al. Sleep drives metabolite clearance from the adult brain. Science 342, 373–377 (2013).
8. Miao, A. et al. Brain clearance is reduced during sleep and anesthesia. Nat. Neurosci. 27, 1046–1050 (2024).
9. Fultz, N. E. et al. Coupled electrophysiological, hemodynamic, and cerebrospinal fluid oscillations in human sleep. Science 366, 628–631 (2019).
10. Ding, X. B. et al. Impaired meningeal lymphatic drainage in patients with idiopathic Parkinson's disease. Nat. Med. 27, 411–418 (2021).
11. Zou, W. et al. Blocking meningeal lymphatic drainage aggravates Parkinson's disease-like pathology in mice overexpressing mutated alpha-synuclein. Transl. Neurodegener. 8, 7 (2019).
12. Taoka, T. et al. Evaluation of glymphatic system activity with the diffusion MR technique: diffusion tensor image analysis along the perivascular space (DTI-ALPS) in Alzheimer's disease cases. Jpn. J. Radiol. 35, 172–178 (2017).
13. McKnight, C. D. et al. Diffusion along perivascular spaces reveals evidence supportive of glymphatic function impairment in Parkinson disease. Parkinsonism Relat. Disord. 89, 98–104 (2021).
14. Shen, T. et al. Diffusion along perivascular spaces as marker for impairment of glymphatic system in Parkinson's disease. npj Parkinsons Dis. 8, 174 (2022).
15. Wood, K. H. et al. Diffusion tensor imaging-along the perivascular-space index is associated with disease progression in Parkinson's disease. Mov. Disord. 39, 1504–1513 (2024).
16. Park, Y. W. et al. Magnetic resonance imaging-visible perivascular spaces in basal ganglia predict cognitive decline in Parkinson's disease. Mov. Disord. 34, 1672–1679 (2019).
17. Donahue, E. K. et al. Global and regional changes in perivascular space in idiopathic and familial Parkinson's disease. Mov. Disord. 36, 1126–1136 (2021).
18. Han, F. et al. Reduced coupling between cerebrospinal fluid flow and global brain activity is linked to Alzheimer disease-related pathology. PLoS Biol. 19, e3001233 (2021).
19. Han, F. et al. Decoupling of global brain activity and cerebrospinal fluid flow in Parkinson's disease cognitive decline. Mov. Disord. 36, 2066–2076 (2021).
20. Wang, Z. et al. Reduced coupling of global brain function and cerebrospinal fluid dynamics in Parkinson's disease. J. Cereb. Blood Flow Metab. 43, 1328–1339 (2023).

21. Mossige, I. et al. Comparing glymphatic function measures: diffusion tensor image analysis along perivascular spaces (DTI-ALPS) versus intrathecal contrast-enhanced MRI. Radiology 318, e252070 (2026).
22. Schilling, K. G. et al. White matter geometry confounds diffusion tensor imaging along perivascular space (DTI-ALPS) measures. Hum. Brain Mapp. 46, e70282 (2025).
23. Bjerknes, S., Skogseid, I. M., Hauge, T. J., Dietrichs, E. & Toft, M. Subthalamic deep brain stimulation improves sleep and excessive sweating in Parkinson's disease. npj Parkinsons Dis. 6, 29 (2020).
24. Zuzuárregui, J. R. P. & Ostrem, J. L. The impact of deep brain stimulation on sleep in Parkinson's disease: An update. J. Parkinsons Dis. 10, 393–404 (2020).
25. Wardlaw, J. M. et al. Perivascular spaces in the brain: anatomy, physiology and pathology. Nat. Rev. Neurol. 16, 137–153 (2020).
26. Postuma, R. B. et al. MDS clinical diagnostic criteria for Parkinson's disease. Mov. Disord. 30, 1591–1601 (2015).
27. Bronstein, J. M. et al. Deep brain stimulation for Parkinson disease: an expert consensus and review of key issues. Arch. Neurol. 68, 165 (2011).
28. World Medical Association. World medical association declaration of helsinki: ethical principles for medical research involving human subjects. JAMA 310, 2191–2194 (2013).
29. Tomlinson, C. L. et al. Systematic review of levodopa dose equivalency reporting in Parkinson's disease. Mov. Disord. 25, 2649–2653 (2010).
30. Goetz, C. G. et al. Movement Disorder Society-sponsored revision of the Unified Parkinson's Disease Rating Scale (MDS-UPDRS): scale presentation and clinimetric testing results. Mov. Disord. 23, 2129–2170 (2008).
31. Hoehn, M. M. & Yahr, M. D. Parkinsonism: onset, progression and mortality. Neurology 17, 427–442 (1967).
32. Chaudhuri, K. R. et al. The metric properties of a novel non-motor symptoms scale for Parkinson's disease: results from an international pilot study. Mov. Disord. 22, 1901–1911 (2007).
33. Jenkinson, C., Fitzpatrick, R., Peto, V., Greenhall, R. & Hyman, N. The Parkinson's disease questionnaire (PDQ-39): development and validation of a Parkinson's disease summary index score. Age Ageing 26, 353–357 (1997).
34. Folstein, M. F., Folstein, S. E. & McHugh, P. R. "Mini-mental state". A practical method for grading the cognitive state of patients for the clinician. J. Psychiatr. Res. 12, 189–198 (1975).
35. Hamilton, M. A rating scale for depression. J. Neurol. Neurosurg. Psychiatry 23, 56–62 (1960).
36. Hamilton, M. The assessment of anxiety states by rating. Br. J. Med. Psychol. 32, 50–55 (1959).
37. Chaudhuri, K. R. et al. The Parkinson's disease sleep scale: a new instrument for assessing sleep and nocturnal disability in Parkinson's disease. J. Neurol. Neurosurg. Psychiatry 73, 629–635 (2002).

38. Tustison, N. J. et al. N4ITK: improved N3 bias correction. IEEE Trans. Med. Imaging 29, 1310–1320 (2010).
39. Fischl, B. FreeSurfer. Neuroimage 62, 774–781 (2012).
40. Reuter, M., Schmansky, N. J., Rosas, H. D. & Fischl, B. Within-subject template estimation for unbiased longitudinal image analysis. Neuroimage 61, 1402–1418 (2012).
41. Avants, B. B., Epstein, C. L., Grossman, M. & Gee, J. C. Symmetric diffeomorphic image registration with cross-correlation: evaluating automated labeling of elderly and neurodegenerative brain. Med. Image Anal. 12, 26–41 (2008).
42. Jenkinson, M., Beckmann, C. F., Behrens, T. E. J., Woolrich, M. W. & Smith, S. M. FSL. Neuroimage 62, 782–790 (2012).
43. Power, J. D., Barnes, K. A., Snyder, A. Z., Schlaggar, B. L. & Petersen, S. E. Spurious but systematic correlations in functional connectivity MRI networks arise from subject motion. Neuroimage 59, 2142–2154 (2012).
44. Andersson, J. L. R. & Sotiropoulos, S. N. An integrated approach to correction for off-resonance effects and subject movement in diffusion MR imaging. Neuroimage 125, 1063–1078 (2016).
45. Basser, P. J., Mattiello, J. & LeBihan, D. MR diffusion tensor spectroscopy and imaging. Biophys. J. 66, 259–267 (1994).
46. Sepehrband, F. et al. Image processing approaches to enhance perivascular space visibility and quantification using MRI. Sci. Rep. 9, 12351 (2019).

Figures

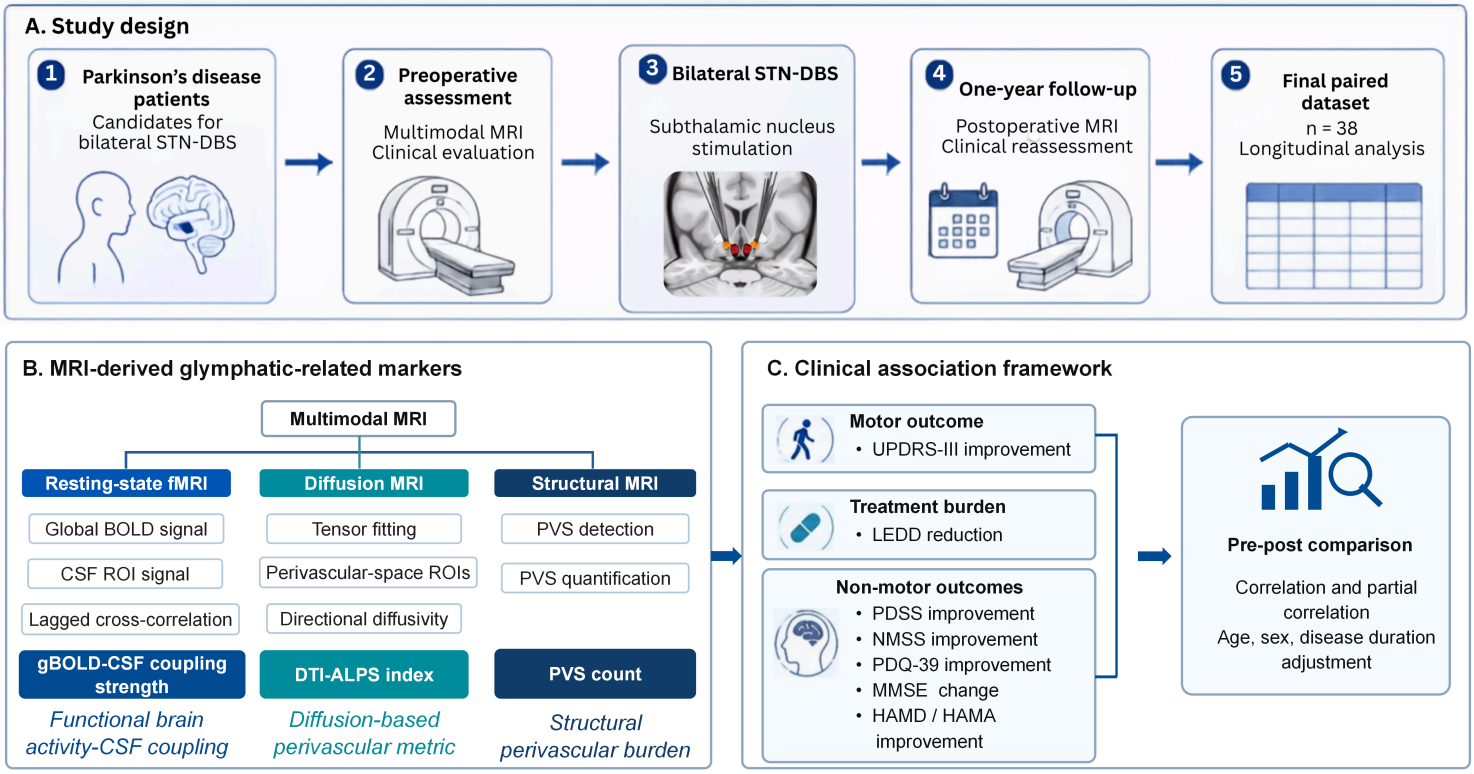


Figure 1

Study design and multimodal MRI framework for evaluating glymphatic-related changes after STN-DBS.

A, Overview of the longitudinal study design. Patients with Parkinson's disease who were candidates for bilateral subthalamic nucleus deep brain stimulation underwent preoperative multimodal MRI and clinical assessment, followed by bilateral STN-DBS and one-year postoperative reassessment. The final paired cohort included 38 patients for longitudinal analysis. B, MRI-derived glymphatic-related markers. Resting-state fMRI was used to quantify gBOLD-CSF coupling strength. Diffusion MRI was used to calculate the DTI-ALPS index, and structural MRI was used for PVS burden. C, Clinical association framework. Longitudinal MRI changes were related to motor outcomes, treatment burden, and non-motor outcomes using pre-post comparisons, correlation analyses.

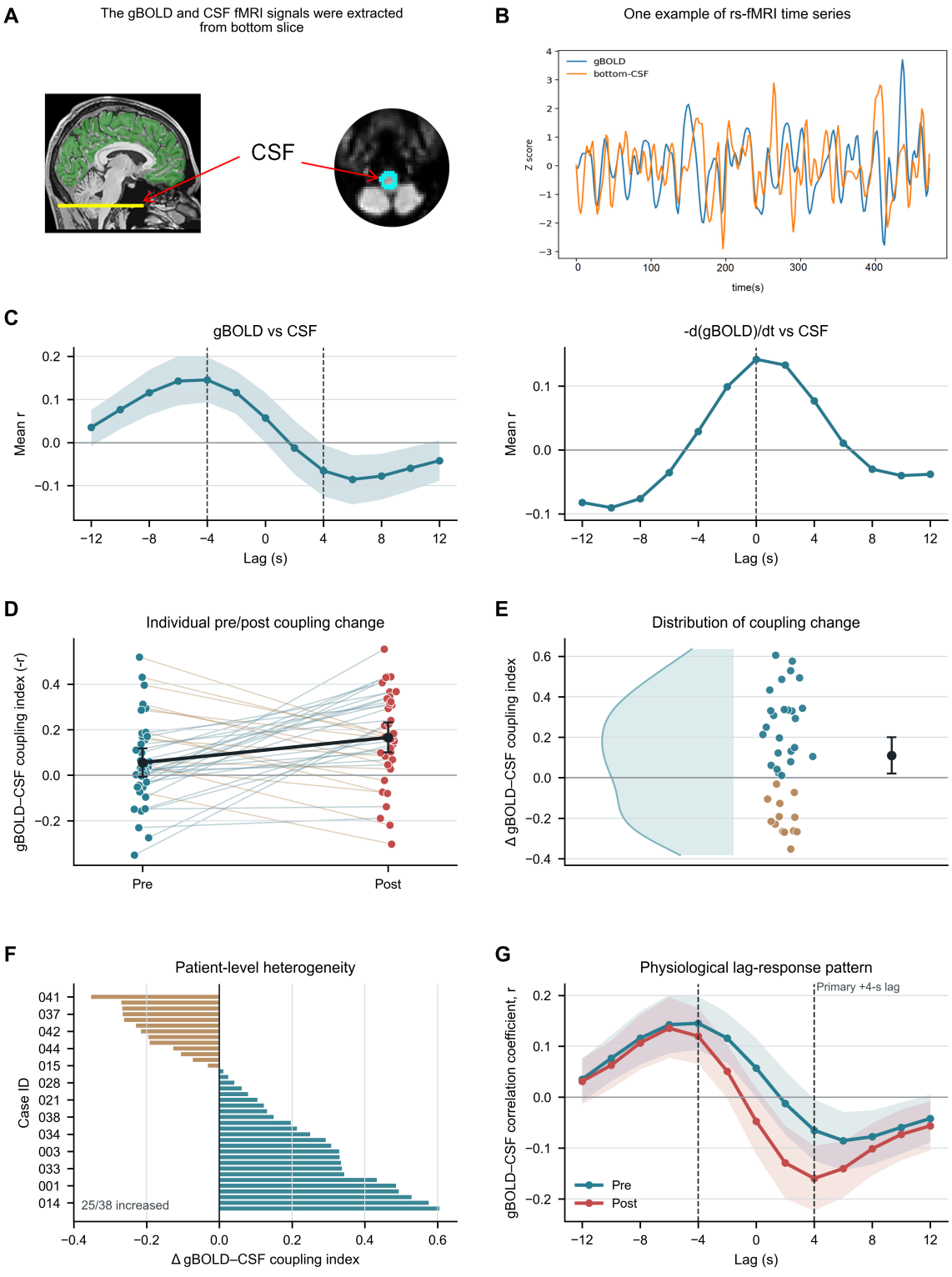


Figure 2

Longitudinal change in gBOLD-CSF coupling after STN-DBS.

A-C, Resting-state fMRI was used to extract global BOLD and bottom-slice CSF signals. Representative normalized time series are shown together with lagged correlation analyses between gBOLD and CSF signals, including the derivative-based coupling pattern using −d(gBOLD)/dt.

D, Individual pre and postoperative gBOLD-CSF coupling index values. Dots represent individual patients, paired lines indicate within-subject longitudinal changes, and black markers with error bars denote the group mean and 95% confidence interval. E, Distribution of postoperative change in gBOLD-CSF coupling index, calculated as post minus pre. The violin plot shows the overall distribution, dots show individual patients, and the black point with error bar indicates the mean change and 95% confidence interval. F, Patient-level heterogeneity in coupling change, sorted by individual ΔgBOLD-CSF coupling index. Positive values indicate postoperative coupling enhancement. G, Physiological lag-response pattern of gBOLD-CSF correlation before and after STN-DBS. Lines show mean correlation coefficients across temporal lags, with shaded areas indicating 95% confidence intervals. The +4-s lag was prespecified as the primary analysis point.

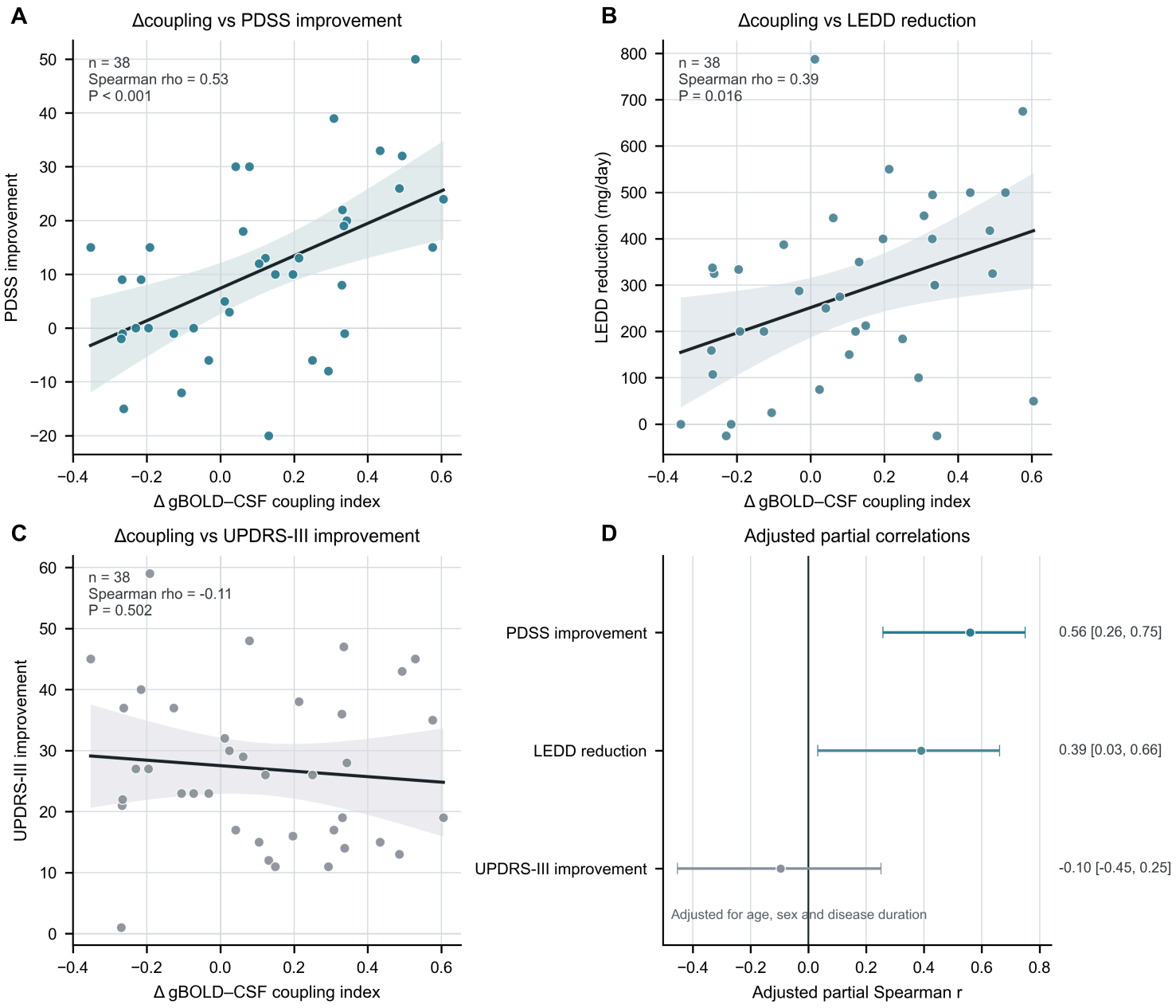


Figure 3

Clinical relevance of postoperative gBOLD-CSF coupling enhancement.

A, Association between postoperative change in gBOLD-CSF coupling index and PDSS improvement in all patients. Greater coupling enhancement was associated with larger PDSS improvement. B, Association between postoperative change in gBOLD-CSF coupling index and LEDD reduction. C, Association between postoperative change in gBOLD-CSF coupling index and UPDRS-III improvement. No significant association was observed. D, Adjusted partial Spearman correlations between coupling enhancement and clinical outcomes after controlling for age, sex, and disease duration. Error bars indicate 95% bootstrap confidence intervals.

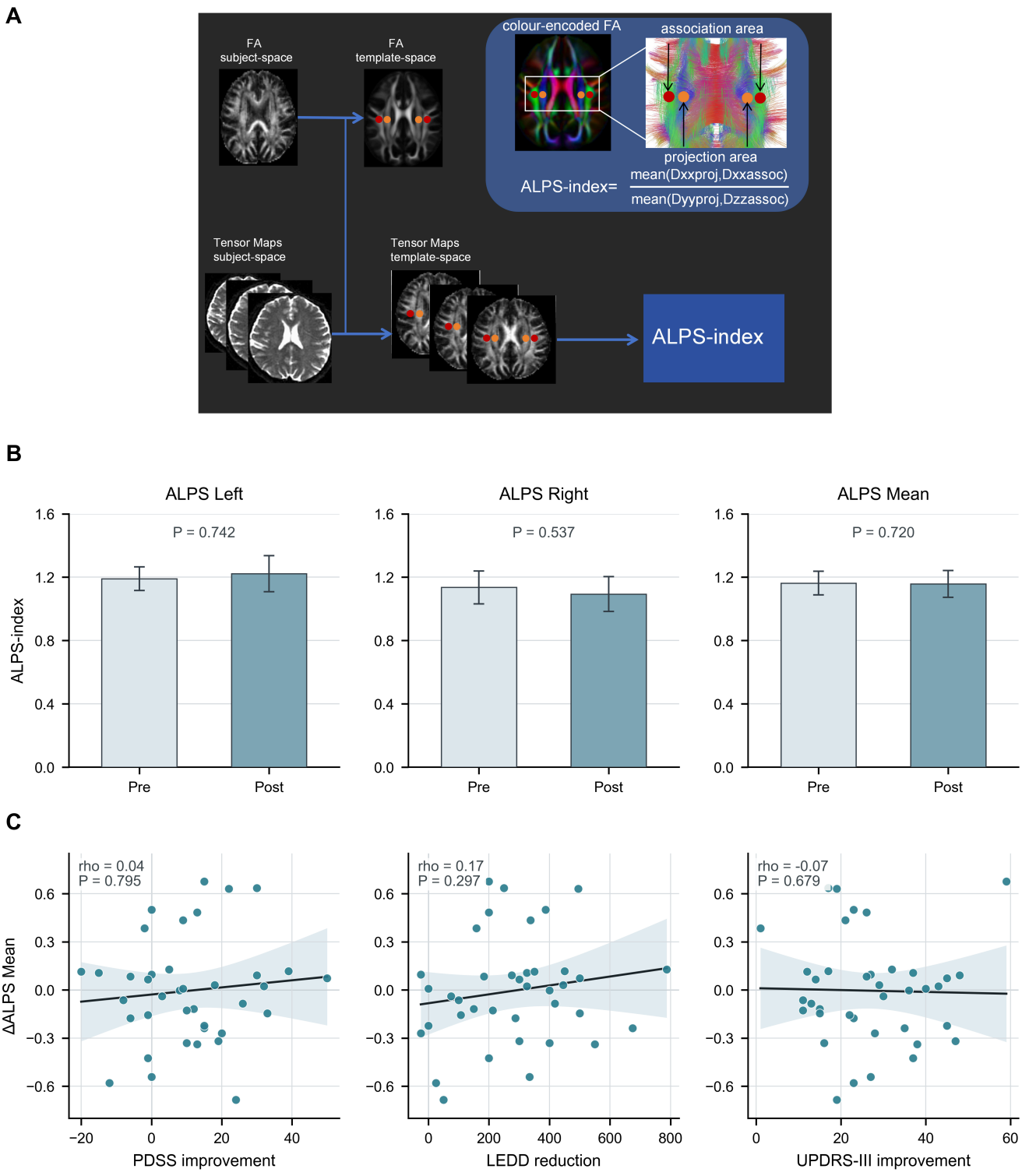


Figure 4

Longitudinal changes in DTI-ALPS after STN-DBS.

A, Schematic representation of the DTI-ALPS index calculation. Diffusion tensor maps were transformed from subject space to template space, and diffusivity values were sampled from projection and association fiber regions to derive the ALPS index. B, Pre and postoperative DTI-ALPS index values for

the left hemisphere, right hemisphere, and bilateral mean in all patients (Wilcoxon P). C, Associations between change in ALPS Mean and clinical outcomes, including PDSS improvement, LEDD reduction, and UPDRS-III improvement.

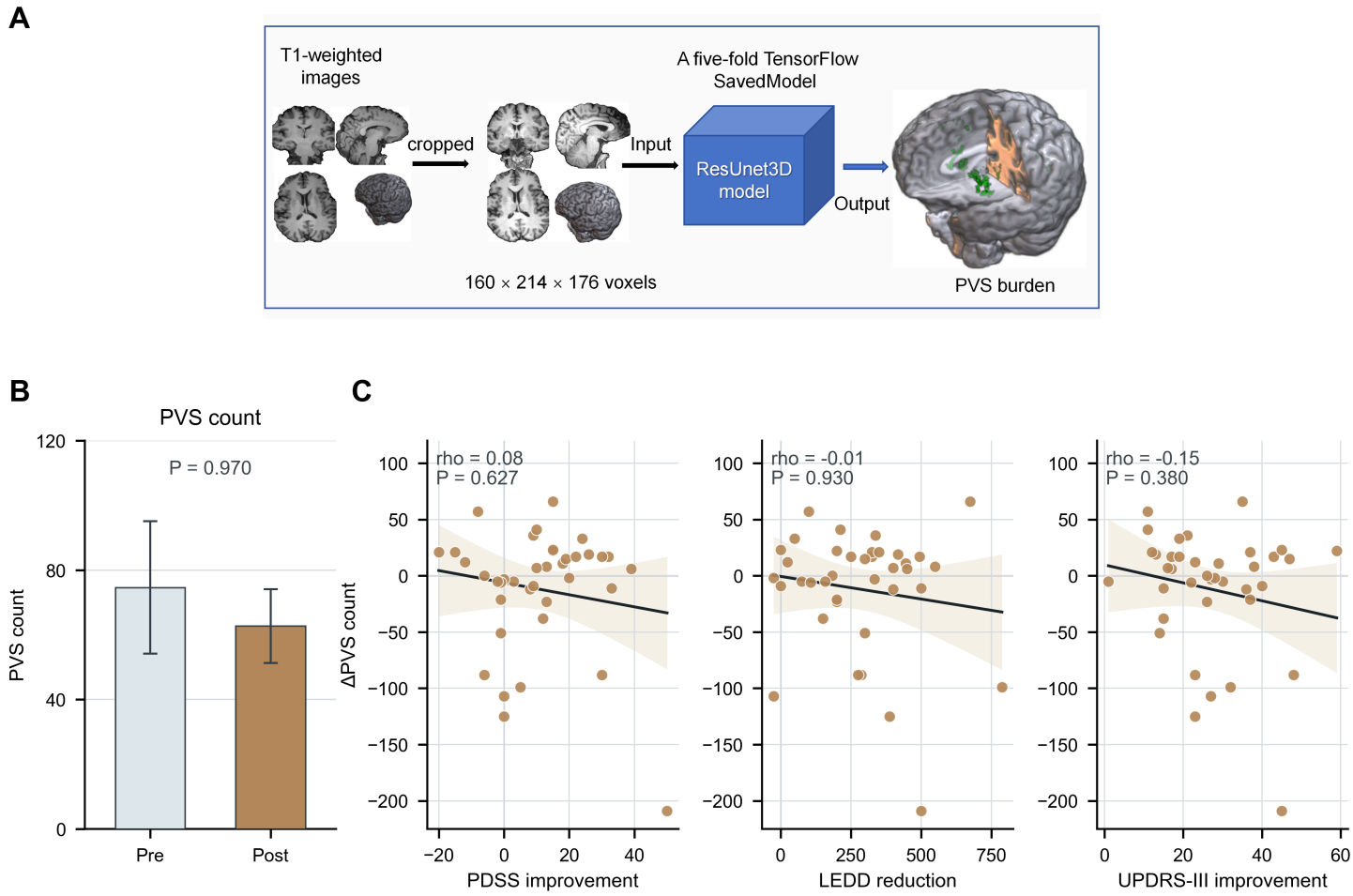


Figure 5

Longitudinal changes in PVS burden after STN-DBS.

A, Automated PVS segmentation and quantification workflow. T1-weighted images were cropped and processed using a five-fold ResUNet3D model to generate PVS burden estimates. B, Pre and postoperative PVS count in all patients. C, Associations between change in PVS count and clinical outcomes.

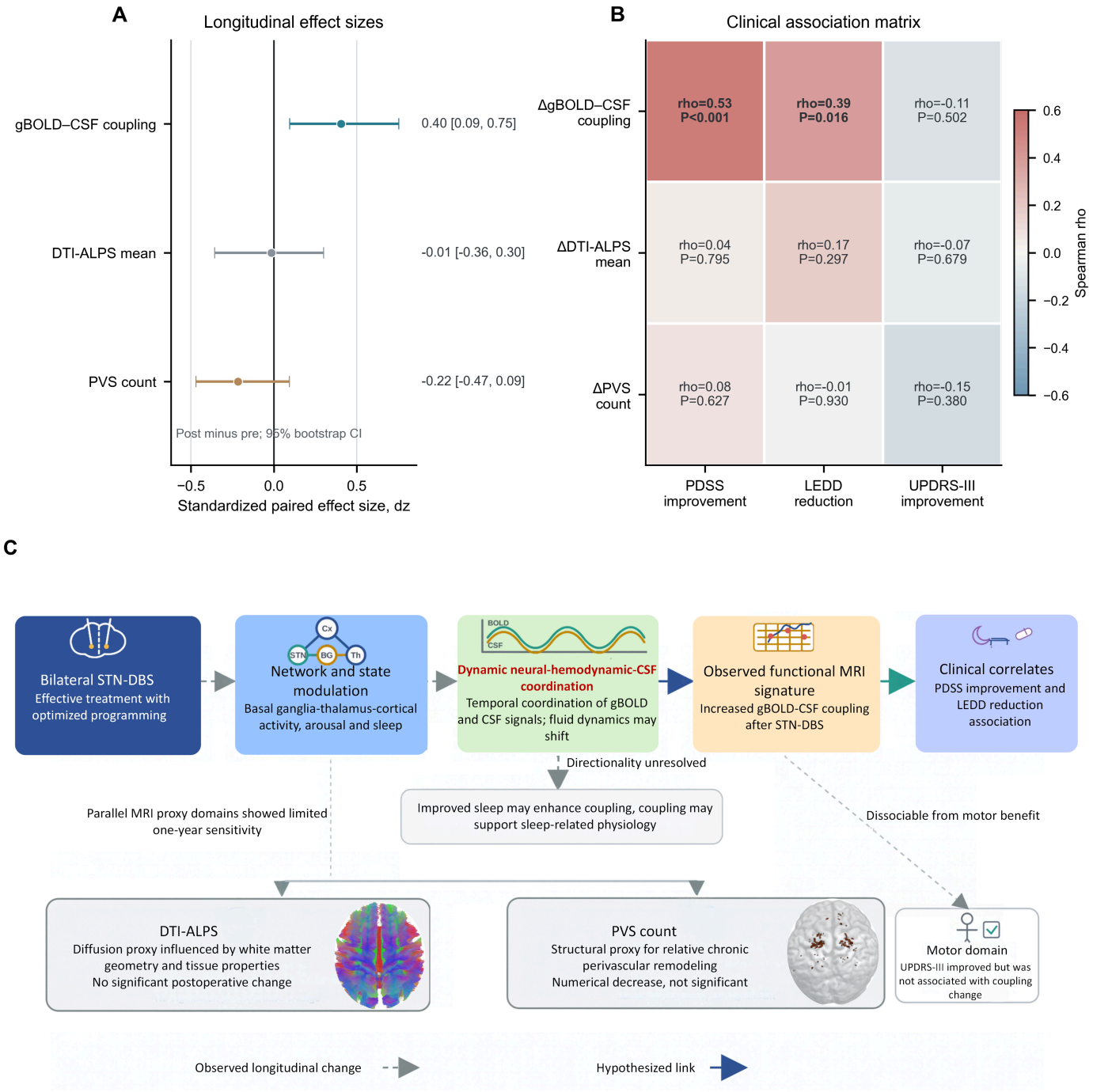


Figure 6

Integrated multimodal signature of glymphatic-related MRI changes and proposed mechanistic framework after STN-DBS.

A, Forest plot showing standardized paired effect sizes for longitudinal changes in gBOLD-CSF coupling, DTI-ALPS mean, and PVS count in all patients. B, Heatmap summarizing Spearman correlations between

changes in glymphatic-related MRI markers and clinical outcomes. C, Proposed mechanistic framework linking STN-DBS to glymphatic-related MRI changes. STN-DBS may modulate basal ganglia-thalamocortical and sleep-arousal states, thereby altering the temporal coordination of global BOLD activity and CSF signals. The observed increase in gBOLD-CSF coupling and its association with PDSS improvement support a dynamic functional pathway. DTI-ALPS and PVS count showed limited one-year change, consistent with diffusion and structural readouts that may be slower, less specific, or less sensitive to state-dependent physiology. Solid arrows indicate findings supported by the present dataset; dashed arrows indicate plausible but unproven links. The figure does not imply restored glymphatic clearance or a causal pathway.

Supplementary Files

This is a list of supplementary files associated with this preprint. Click to download.

- SupplementaryMethods.docx
- SupplementaryTables.docx